

# EVALUATION OF PINHOLE CAMERA RESOLUTION FOR NSLS-II STORAGE RING \*

I. Pinayev <sup>#</sup>, NSLS-II Project, BNL, Upton, NY 11973, U.S.A.

## Abstract

The NSLS-II Storage Ring will provide ultrabright radiation sources with extra-small sizes of the circulating electron beam. The beam dimensions will be monitored with a pinhole camera. In this paper we discuss the possible design and ultimate achievable resolution of the system. Modeling is based on the SRW code as well as numerical calculations using MATLAB.

## INTRODUCTION

The pinhole camera has been a workhorse for measuring electron beam size on the storage ring-based light sources since it was first utilized at ESRF [1]. The NSLS-II storage ring will utilize an electron beam with diffraction limited source size in the vertical plane [2] in order to achieve unprecedented brightness. The goal of the study described in this paper is to define parameters that most affect resolution of the imaging system and optimize beamline design.

## BEAMLINE LAYOUT

The expected layout of the pinhole camera beamline is shown in Fig. 1. The bending dipoles of the storage ring have low magnetic field of 0.4 T in order to reach small horizontal emittance [2]. Therefore the expected critical energy of the dipole synchrotron radiation is rather low, namely 2.4 keV. To improve resolution by utilizing a shorter wavelength we will employ a three-pole wiggler as a source. The field of the central pole is 1.14 T, the critical photon energy is 6 keV, and the useful synchrotron radiation spectrum extends to 50 keV. The electron beam parameters at the location of the three-pole wiggler are  $\eta_x=0.17$  m,  $\beta_x=4.1$  m, and  $\beta_y=19.3$  m. Taking emittances  $\epsilon_x=1$  nm and  $\epsilon_y=8$  pm and relative energy spread  $\sigma_E/E=0.1\%$  one can easily find the transverse dimensions of the source:  $\sigma_x=180$  microns (defined mostly by energy spread) and  $\sigma_y=12.4$  microns.

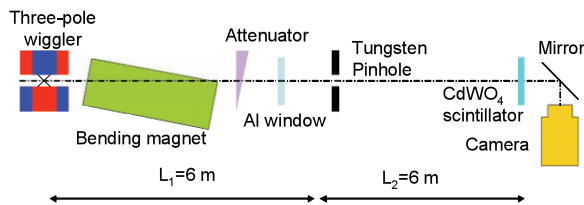


Fig.1 Layout of the pinhole camera beamline.

The first element of the pinhole camera beamline is a variable filter/attenuator. It constitutes a wedge, mounted on a linear actuator to set desirable transmission level.

The filter serves two functions: the first is to bring intensity down to an acceptable level. The second function is to suppress long-wavelength radiation, in order to improve resolution. The filter is followed by an aluminum window so synchrotron radiation can exit to the atmosphere. Usually the material of the wedge is copper but we found it unsuitable due to substantial transmission of low-energy photons (Fig. 2).

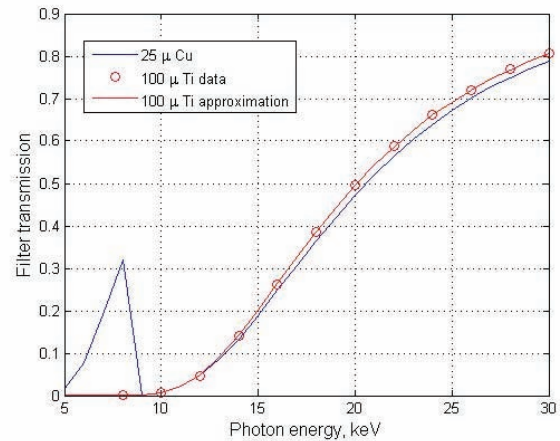


Fig. 2. Transmission curves for 25 microns of copper and 100 microns of titanium. Data from [4].

For our design we plan to use titanium, which does not have absorption lines in the spectral range of interest and has excellent vacuum compatibility. The Ti filter transmission curve also is shown in Fig. 2. Fig. 3 shows on-axis brightness of a three-pole wiggler source after being filtered by 50 microns of titanium.

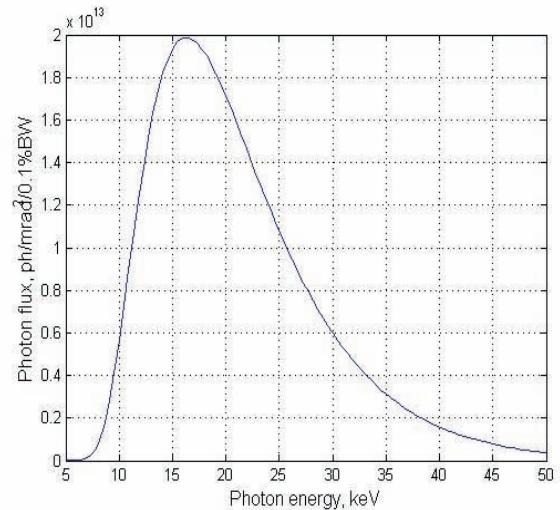


Fig. 3. Spectral brightness of the three-pole wiggler source after a 50 micron Ti filter.

\*Work supported by the U.S. Department of Energy with Contract No. DE-AC02-98CH10886

<sup>#</sup>pinayev@bnl.gov

The 100 micron aluminum window provides sufficient mechanical strength and has substantial transmission above 10 keV (Fig. 4). Because all low-energy photons are absorbed by the filter, the thermal load on the window is about 0.3 W/mm<sup>2</sup>.

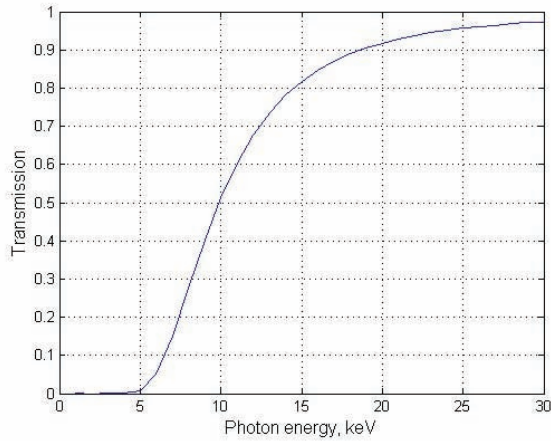


Fig. 4 Transmission of aluminum window 100 microns thick.

The pinhole installed after the aluminum window will be made of tungsten and will have fixed size (we will consider usage of variable pinhole, as well). Putting the pinhole assembly outside the vacuum chamber simplifies the design and service of the beamline. The distance from the pinhole to the source is defined by available physical space and is expected to be approximately 6 meters. The image of the electron beam will be observed with CdWO<sub>4</sub> phosphor and a camera equipped with a zoom lens.

### SIMULATIONS

In our simulations we assumed a 6 meter distance from the source to the pinhole, and the same distance from the pinhole to the phosphor screen. We disregarded the loss of resolution in the phosphor screen and optical imaging system, thus concentrating on the fundamental factors affecting resolution.

For specified photon energy one can easily find the resolution of a pinhole camera using SRW code [5]. However, in our case the source has a continuous (and quite wide) spectral range. To handle such a situation it is possible to find profiles of photon flux for multiple wavelengths and then perform summing, but this is quite labor extensive. We chose a different approach. The effective resolution of the system at particular wavelengths was estimated using natural units  $u = \sqrt{\lambda L_1 L_2 / (L_1 + L_2)}$  and  $v = \sqrt{\lambda (L_1 + L_2) L_2 / L_1}$  introduced in [6]. Well-known analytical solutions exist for small apertures (Fraunhofer diffraction) as well as for large ones (geometric shadow). The curve (E) for monochromatic Fresnel diffraction shown in Fig. 13 in [6] was approximated using the formula below:

$$\sigma = v \sqrt{u^2/8 + 0.13/u^2} \cdot \left[ 1 - \frac{0.476}{1 + ((\ln u - 0.385)/0.341)^2} \right]$$

The first term is a quadrature sum of the width of resolutions due to geometric shadow and Fraunhofer diffraction. The term in square brackets is a correction multiplier accounting for Fresnel diffraction. Such fit provides good agreement with SRW calculations as well. The fit curve is shown in Fig. 5.

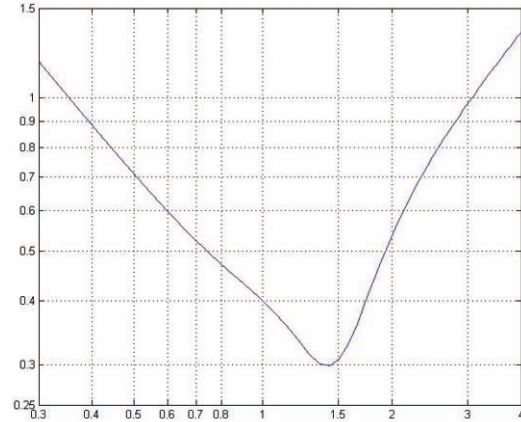


Fig. 5. Effective resolution of pinhole camera in natural units.

To estimate photon flux on the phosphor we needed also to calculate the spectral density of synchrotron radiation from the three-pole wiggler. For this we used a well-known formula for synchrotron radiation from a bending magnet:

$$\frac{dN}{d\Omega} [photons/sec/mrad^2] = 1.325 \times 10^{16} \frac{\Delta\omega}{\omega} E^2 [GeV] \cdot I[A] \left(\frac{\lambda}{\lambda_c}\right)^2 K_{2/3}^2 \left(\frac{\lambda}{2\lambda_c}\right)$$

The spectrum was multiplied by the transmission coefficients of the filter and aluminum window. In order to evaluate the attenuation of the titanium filter, the penetration depth of X rays was approximated with the following formula:

$$\lambda [\mu m] = 0.0157 E_{hv}^3 + 0.04221 E_{hv}^2,$$

and for aluminum

$$\lambda_{Al} [\mu m] = 0.0740 E_{hv}^3 + 0.0944 E_{hv}^2.$$

where E<sub>hv</sub> is photon energy in keV.

In the dedicated MATLAB® script, numerical integration over the spectral range from 6 to 50 keV was performed in order to estimate photon density on the phosphor screen. For each particular wavelength, the number of photons that passed through the pinhole was found, and photon density in the image plane was calculated using a Gaussian curve which width corresponds to resolution. The point spread function was found by summing over all wavelengths (such as shown in Fig. 6) and was fitted with a Gaussian curve. The

resulting effective width was used as the resolution of the system.

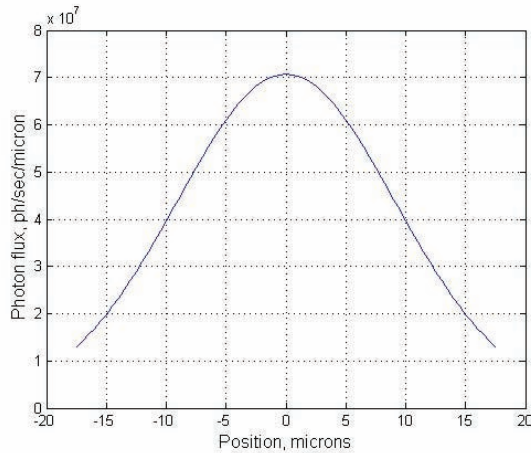


Fig. 6. Point spread function in phosphor plane for 20 microns pinhole and 120 micron Ti filter.

To optimize the design the described procedure was applied to the set of pinhole sizes and filter thicknesses. The 3D curve for calculated resolution dependence on filter thickness and pinhole size is shown in Fig. 7.

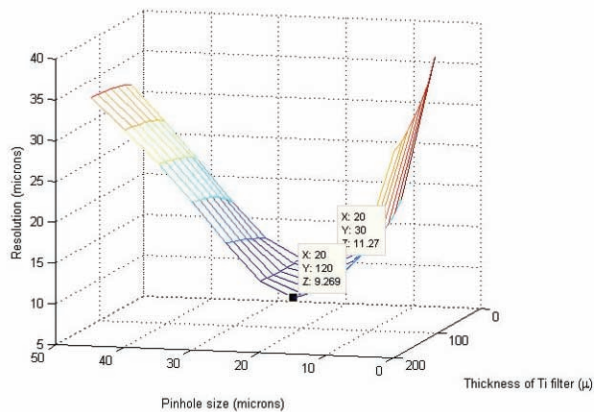


Fig. 7. Dependence of pinhole camera resolution on aperture size and thickness of Ti filter.

The best resolution is achieved with a pinhole of about 20 microns and has weak dependence on the thickness of the filter. The resolution of the system is slightly below r.m.s. vertical beam size but is certainly suitable for measuring the horizontal beam size.

To verify calculations we used SRW to generate 2D profiles of photon flux at the image plane with 20 micron pinhole and 50 micron filter at different wavelengths. Summing the intensities gave us total photon flux density and therefore the profile of the image of a realistic electron beam. The resulting image is shown in Fig. 8. There is excellent agreement between the SRW simulation and the approximations used in this paper.

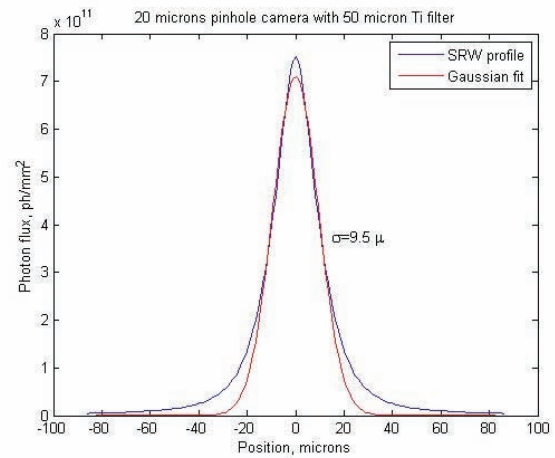


Fig. 8. Point spread function of pinhole camera obtained by summing of photon beam profiles generated by SRW.

To improve resolution we estimated a solution where a pinhole will be placed in the vacuum chamber in place of a crotch absorber. In such a situation distance from the pinhole to the source is 3 meters and it is easy to obtain 5-fold magnification by placing a fluorescent screen 15 meters from the pinhole. The results of the simulations are shown in Fig. 9.

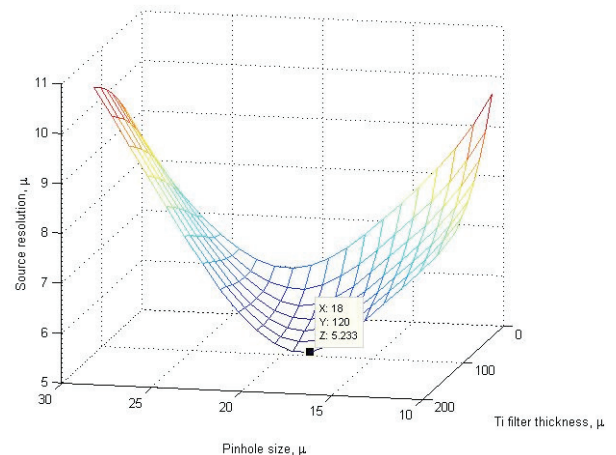


Fig. 9. Resolution of pinhole camera with 5-fold magnification.

The proposed design improves resolution by a factor of 2 and makes the pinhole camera suitable for measuring vertical beam size. Also, due to the magnification, the resolution of the imaging system is of less concern. However, there are certain technical difficulties, such as provisions for adjusting the pinhole, which need to be overcome.

## CONCLUSIONS

The pinhole camera planned for installation on the NSLS-II storage ring will not have sufficient resolution for robust measurement of vertical beam size if it is positioned outside the vacuum chamber, but the camera can be a useful tool for monitoring fluctuations of beam

emittance during regular operations. If the pinhole will replace a crotch absorber inside dipole vacuum chamber then the required resolution can be achieved.

The resolution in the horizontal plane is quite adequate in both cases and the camera can be very useful for monitoring beam energy spread, which defines the beam size at location of the three-pole wiggler.

### NOTICE

This manuscript has been co-authored by employees of Brookhaven Science Associates, LLC under Contract No. DE-AC02-98CH10886 with the U.S. Department of Energy. The publisher by accepting the manuscript for publication acknowledges that the United States Government retains a non-exclusive, paid-up, irrevocable, world-wide license to publish or reproduce the published form of this manuscript, or allow others to do so, for United States Government purposes.

### REFERENCES

- [1] P. Elleaume et al., J. Synchrotron Rad. (1995). 2, 209-214.
- [2] S. Ozaki et al., "Philosophy for NSLS-II design with sub-nanometer horizontal emittance," PAC'07, pp. 77-79 (2007).
- [3] NSLS-II Preliminary Design Report, available at <http://www.bnl.gov/nsls2/project/PDR>
- [4] "X-ray Filter Transmission" available at [http://henke.lbl.gov/optical\\_constants/filter2.html](http://henke.lbl.gov/optical_constants/filter2.html).
- [5] O. Chubar and P. Elleaume, "Accurate and Efficient Computation of Synchrotron Radiation in the Near Field Region" EPAC98, THP01G, pp.1177-1179.
- [6] B. Yang, "Optical System Design for High-Energy Particle Beam Diagnostics," BIW'02, AIP Proc. 648, 2002, pp.59-78